PHOTONICS Research

Real-time dynamics of soliton triplets in fiber lasers

Yiyang Luo,[1,2,†,*] Ran Xia,[1,2,3,†] Perry Ping Shum,[1,2] Wenjun Ni,[1,2] Yusong Liu,[1,2,3] Huy Quoc Lam,[4] Qizhen Sun,[3] Xiahui Tang,[3] and Luming Zhao[3]

[1]CINTRA CNRS/NTU/THALES, UMI 3288, Research Techno Plaza, 50 Nanyang Drive, Singapore 637553, Singapore
[2]School of Electrical and Electronic Engineering, Nanyang Technological University, Singapore 639798, Singapore
[3]School of Optical and Electronic Information & Wuhan National Laboratory for Optoelectronics, Huazhong University of Science and Technology, Wuhan 430074, China
[4]Temasek Laboratories @ NTU, Research Techno Plaza, 50 Nanyang Drive, Singapore 637553, Singapore
*Corresponding author: luoyy@ntu.edu.sg

Received 10 January 2020; revised 23 March 2020; accepted 2 April 2020; posted 2 April 2020 (Doc. ID 387438); published 14 May 2020

The evolution of soliton molecules emphasizes the complex soliton dynamics akin to matter molecules. Beyond the simplest soliton molecule—a soliton pair constituted by two bound pulses—soliton molecules with more constituents have more degrees of freedom because of the temporal pulse separations and relative phases. Here we detailedly characterize the transient dynamics of soliton triplets in fiber lasers by using the dispersive Fourier transform measurement. A particular form of leading, central, and tailing pulses is constructed to shed new light on more intriguing scenarios and fuel the molecular analogy. Especially the vibrating dynamics of the central and tailing pulses are captured near the regime of equally spaced soliton triplets, which is reminiscent of the recurrent timing jitters within multi-pulse structures. Further insights enable access into a universal form of unequally spaced soliton triplets interpreted as 2 + 1 soliton molecules. Different binding strengths of intramolecular and intermolecular bonds are validated with respect to the diverse internal motions involved in this soliton triplet molecule. All these findings unveil the transient dynamics with more degrees of freedom as well as highlight the possible application for all-optical bit storage.

https://doi.org/10.1364/PRJ.387438

1. INTRODUCTION

Solitons as localized wave structures have attracted considerable attention in a variety of conservative and dissipative nonlinear systems such as fluids, plasma physics, Bose–Einstein condensates, and optics [1–4]. Viewed as the most universal notion, dissipative solitons are involved with a composite balance between dispersion/diffraction and nonlinearity, gain, and loss [5]. As an optimal experimental platform, passively mode-locked fiber lasers not only deliver ultrashort pulses but also uncover plentiful landscapes of dissipative soliton dynamics [6]. In particular, the peak-power clamping-effect-induced multi-pulsing operation [7] is an intensive topic of research for both the scientific interest in mutual interaction dynamics of ultrashort pulses and the promising applications of high-level modulation formats for optical communications and all-optical bit storage [8–10]. Among these multi-pulsing solutions, self-organization-endowed soliton molecules, also termed bound states, have been highlighted with remarkable properties in the analogy of matter molecules [11–14]. Considering the dissipation of the laser system, soliton molecules are of inelastic nature and maintain their patterns in the presence of continuous energy supply. Apart from the stationary solution [15–18], matter molecules also draw some striking analogical scenarios of dynamic manners in soliton molecules. Numerical simulations show that the intramolecular temporal separations and relative phases can evolve along round-trips, which is interpreted as the internal motion of soliton molecules [19–22]. Restricted by the traditional measurements, previous experimental investigations only present the time-averaged results such as the deformed spectral interferograms or autocorrelation traces. Direct investigations of the evolution process are weakly supported by the time-averaged measurement. Hence, it is of great significance to gain access to the transient dynamics of soliton molecules with real-time techniques.

More recently, rapid progress in dispersive Fourier transform (DFT) measurement yields the real-time spectral recordings of ultrashort pulses [23–26]. Shot-to-shot spectral views open new opportunities for transient dynamics such as the birth of mode-locking [27–31], soliton explosion [32,33], soliton pulsation [34–36], and soliton trapping [37]. In addition, the consecutive spectral interferograms of soliton molecules also enable access to their internal motion, dating back to the pioneering work in 2017 [38]. For the most fundamental level of bi-soliton

molecules that are soliton pairs, both the entire build-up process and the transient dynamics are profoundly revealed [39,40]. The degrees of freedom underlying this bi-soliton molecule are the simplex temporal separation and relative phase between the leading pulse and the tailing pulse. It is found that the sliding phase evolution should be ascribed to different phase velocities induced by the intensity difference of the two constituents, while soliton molecule vibration derives from the successive energy flow within the bi-soliton molecule, accompanying the oscillating temporal separation and relative phase [41]. In parallel with the investigations on soliton pairs, soliton molecules with more constituents have more degrees of freedom. They encompass increasing entities and feature complex mutual interplay within molecules. Particularly, bound states of soliton pairs have been investigated for distinguishing the intramolecular and intermolecular bonds, which extends the scope of internal dynamics within a typical 2 + 2 soliton molecular complex [42]. Moreover, soliton triplets have been also highlighted, exhibiting continuous sliding relative phase with fixed temporal separations [41]. Indeed, one more soliton participating in the molecules can reduplicate the degrees of internal motion. Considering the universal form of soliton triplets constituted by leading, central, and tailing pulses, it is desirable to entirely interpret how these particle-like solitons can behave within molecules and further emphasize the analogy with matter physics.

In this paper, we report the first detailed characterization of soliton triplets in a dispersion-managed fiber laser by use of the DFT technique. A particular form of leading, central, and tailing pulses is constructed to shed new light on the increased degrees of internal dynamics. Beyond the stationary state of the equally spaced soliton triplet, one typical finding is the vibrating dynamics of the central and tailing pulses, reminiscent of the recurrent timing jitters within the multilevel modulation formatted unit. With respect to a universal tri-soliton form of unequally spaced soliton triplets, different binding strengths of intramolecular and intermolecular bonds are verified by the diversities of the temporal motion and relative phase evolution.

2. EXPERIMENTAL SETUP

Figure 1(a) depicts the experimental setup, including the near-zero-dispersion passively mode-locked fiber laser and the DFT-based real-time spectral measurement system. In the ring laser cavity, a segment of erbium-doped fiber (EDF, 80 dB/m at 1530 nm, OFS EDF 80) provides the optical gain, which is pumped by a 980 nm laser diode (LD) via a wavelength-division multiplexer (WDM)/isolator hybrid module. This module also ensures the unidirectional oscillation of the fiber laser. A fiber-based polarizer sandwiched by two polarization controllers (PCs) is introduced to initialize the nonlinear polarization rotation (NPR)-based mode-locking. A 90:10 optical coupler (OC) is used to extract the ultrashort pulses from the laser cavity. The total cavity length is around 5.8 m, consisting of 1.5 m long EDF with normal dispersion of +0.061 ps^2/m and 4.3 m long single-mode fiber (SMF) pigtails with anomalous dispersion of −0.022 ps^2/m. The net dispersion is about −0.0031 ps^2 near the zero-dispersion point, and it thus approaches the dispersion-managed soliton regime.

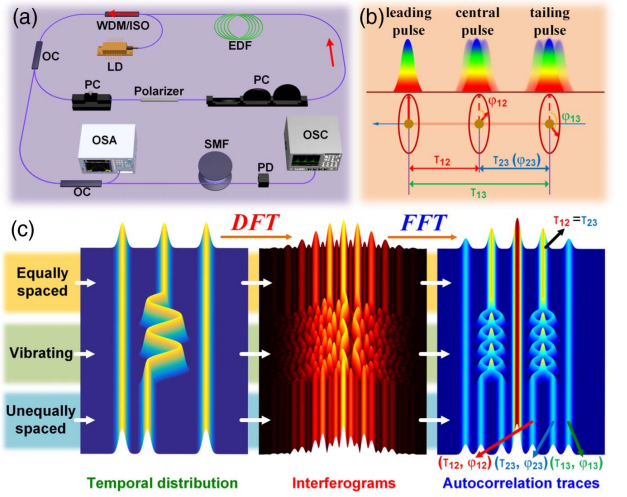

Fig. 1. (a) Schematic diagram of the NPR-based mode-locked fiber laser and the real-time characterization setup; (b) graphical representation of leading, central, and tailing pulses; (c) sketch of the temporal distribution, spectral interferograms, and first-order autocorrelation traces for the equally spaced soliton triplet, vibrating soliton triplet, and unequally spaced soliton triplet. DFT, dispersive Fourier transform; FFT, fast Fourier transform.

Apart from the time-averaged spectral monitoring by an optical spectrum analyzer (OSA), experimental characterization is also captured by the DFT-based real-time spectral measurement. The soliton molecules are stretched in a 15 km SMF with a total dispersion of −330 ps^2 and detected by a high-speed oscilloscope (bandwidth 33 GHz, Agilent) together with a fast photodiode (PD, bandwidth 12 GHz). The spectral interferograms directly recorded by the oscilloscope enable real-time access to the intramolecular dynamics.

Beyond the fundamental bi-soliton molecules, additional solitons can increase the degrees of freedom of the molecules. Phasors distributed along a temporal axis are introduced to represent the soliton molecule with more constituents in recent works, which paves a new way for visualizing the intramolecular dynamics [38]. As presented in Fig. 1(b), a phasor representation is constructed to picture the soliton triplets constituted by leading, central, and tailing pulses. The leading pulse is set as the reference with a fixed pointing direction. The relative positions and pointing directions of the central/tailing pulses respectively feature the temporal separations and relative phases, denoted by the variables (τ, φ). This form shown in Fig. 1(b) illustrates a specific case of the soliton triplet with an equal temporal distribution. This case is a common observation under time-averaged investigations and yields the simple duplication of the bi-soliton molecule. One particular scenario displays the internal motions of the central and tailing pulses that undergo strong interactions within molecules. Figure 1(c) presents the sketch of temporal distribution, spectral interferograms, and autocorrelation traces in three different cases of the stationary equally spaced soliton triplet, vibrating soliton triplet, and unequally spaced soliton triplet. The spectral interferograms can unfold the relative phases within the soliton triplets. The first-order autocorrelation traces are calculated by Fourier

transforming the spectral interferograms. Due to the correlation principle, seven bright fringes are symmetrically located on the autocorrelation trace, respectively representing the variables $(\tau_{12}, \varphi_{12})$, $(\tau_{23}, \varphi_{23})$, and $(\tau_{13}, \varphi_{13})$. Considering the condition $\tau_{12} = \tau_{23}$, the $(\tau_{12}, \varphi_{12})$ and $(\tau_{23}, \varphi_{23})$ fringes will overlap, corresponding to the equally spaced case. Both the temporal separations and the relative phases between each pulse can be retrieved from these fringes. In presence of mutual interactions, the internal dynamics of soliton triplets should be much more plentiful as well as involve some recurrent motion of the central and tailing pulses. Guided by this tri-soliton form, we will experimentally characterize various soliton triplets through analyzing the consecutive spectral interferograms and their calculation results of the shot-to-shot autocorrelation traces.

3. RESULTS AND DISCUSSIONS

A. Stationary Equally Spaced Soliton Triplet

By adjusting the pump strength and the intracavity polarization states, the proposed passively mode-locked fiber laser can approach the dispersion-managed soliton regime due to the near-zero dispersion. This pulse shaping mechanism precludes the formation of Kelly sidebands. The chirping characteristic stretches the pulse within the cavity and thus facilitates the interactions among multiple solitons. With appropriate settings, we prepare a typical soliton triplet constituted by three dispersion-managed solitons. The averaged DFT spectrum (black line) and OSA-measured spectrum (red line) are presented in Fig. 2(a). The two spectra are of good consistency and characterized by superimposed interference modulation fringes. The corresponding pulse train is shown in Fig. 2(b). The pulse interval is ~29 ns, indicating the fundamental mode-locking state. In order to gain insight into the transient dynamics, real-time spectral measurement is implemented to capture each soliton triplet. Figure 2(c) depicts the pulse train after DFT. The shot-to-shot spectral interferograms are 2D contour plotted in Fig. 2(d) with 2000 consecutive round-trips, the inset of which illustrates the close-up from 1565 to 1575 nm. Two sets of interference fringes are observed with the same period of 1.3 nm, and they maintain their structures without any obvious evolving features. By taking the Fourier transform, we obtain the corresponding shot-to-shot first-order autocorrelation traces as presented in Fig. 2(e). Five bright fringes are symmetrically distributed on the 2D contour plot with identical separation, implying that these three dispersion-managed solitons are equally spaced. Furthermore, the temporal separations and relative phases are retrieved from the first-order autocorrelation traces [Figs. 2(f) and 2(g)]. $(\tau_{12}, \varphi_{12})$ and $(\tau_{13}, \varphi_{13})$ remain almost unchanged regardless of the noise background. In consideration of the consistency relations of $\tau_{12} + \tau_{23} = \tau_{13}$ and $\varphi_{12} + \varphi_{23} = \varphi_{13}$, we can conclude that the leading pulse, central pulse, and tailing pulse are mainly phase-locked with an identical intramolecular separation of 6.48 ps. Specially, no obvious temporal motion is observed within the molecules. Hence, this soliton triplet approaches the stationary regime with relatively low intramolecular timing jitters.

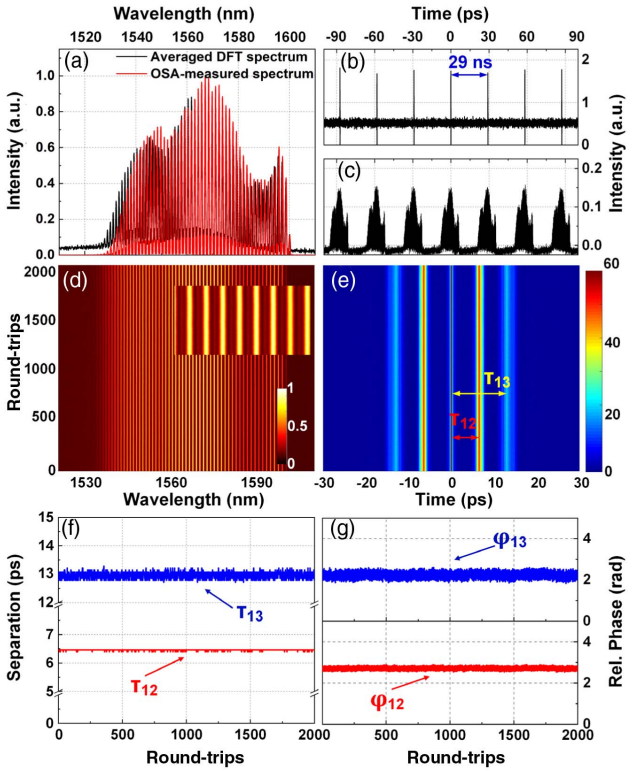

Fig. 2. Stationary equally spaced soliton triplet. (a) Averaged DFT spectrum (black line) and OSA-measured spectrum (red line); (b), (c) pulse trains before and after DFT; (d) 2D contour plot of the shot-to-shot spectra, and the inset shows the close-up; (e) 2D contour plot of the shot-to-shot first-order autocorrelation traces; (f), (g) retrieved temporal separations and relative phases of the central pulse and tailing pulse.

B. Vibrating Soliton Triplet

Vibrating dynamics is a striking property fueling the analogy of soliton and matter molecules. A typical vibrating motion is induced near the regime of the equally spaced soliton triplet. The recorded real-time spectral interferograms and close-up 1 in Figs. 3(a) and 3(c) exhibit obvious oscillating structures arising from the continuous relative phase oscillation. This kind of molecule evolution results in blurred fringes and reduced contrast ratios in the time-averaged spectral recordings. In contrast to the stationary equally spaced soliton triplet, the bright fringes of the shot-to-shot first-order autocorrelation traces [see in Fig. 3(b)] are no longer unchanged, declaring periodic motion of the central pulse and the tailing pulse. In particular, close-up 2 of the fringes, corresponding to the variables $(\tau_{12}, \varphi_{12})$, $(\tau_{23}, \varphi_{23})$, and $(\tau_{13}, \varphi_{13})$ is illustrated in Fig. 3(d). Note that one set of the autocorrelation trace is consistent with two possible solutions. Particularly, the two closely spaced fringes have two corresponding relations between the fringes and variables $(\tau_{12}, \varphi_{12})$ and $(\tau_{23}, \varphi_{23})$. The spectral resolution of the DFT technique imposes on the resolution and contrast of the fringes. Thus, we cannot readily identify both fringes. First, we take one possible solution to investigate the internal motion by retrieving the variable $(\tau_{12}, \varphi_{12})$. The retrieved pulse separations are shown in Fig. 3(e). It is found that the central

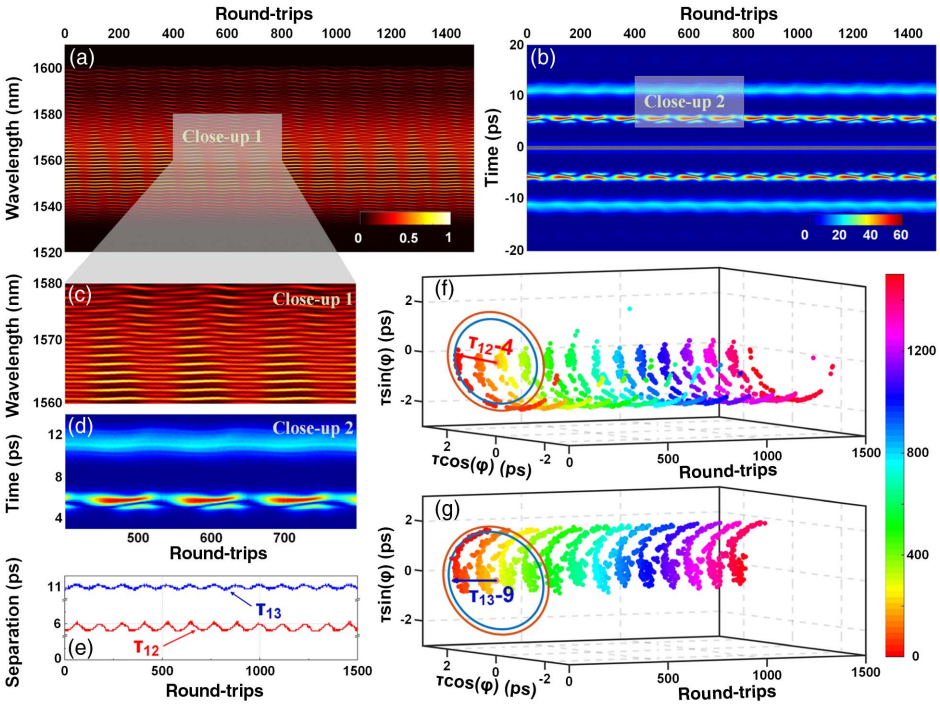

Fig. 3. Vibrating equally spaced soliton triplet. (a) 2D contour plot of the shot-to-shot spectra; (b) 2D contour plot of the shot-to-shot first-order autocorrelation traces; (c), (d) close-ups of the spectra and autocorrelation traces; (e) retrieved temporal separations of the central pulse and tailing pulse; (f), (g) trajectories of $(\tau_{12}, \varphi_{12})$ and $(\tau_{13}, \varphi_{13})$ in the interaction spaces.

pulse and the tailing pulse synchronously approach and deviate from the leading pulse with an identical period of ~115 round-trips, albeit of different oscillation amounts. Visualized insights of the vibrating dynamics can be gained in the 3D plotted interaction spaces as depicted in Figs. 3(f) and 3(g). The trajectories of $(\tau_{12}, \varphi_{12})$ and $(\tau_{13}, \varphi_{13})$ both evolve between two closely spaced orbits with separations of 0.48 ps and 0.32 ps. This intramolecular vibration scenario inherits the similar manners within soliton pairs and further duplicates the degrees of freedom in the sense of more constituents and interactions. Especially, the intensity differences of the leading, central, and tailing pulses dominate the intramolecular evolution. The persistent energy exchange within the soliton triplet leads to a periodic change of their intensities. Thus, the temporal separations and relative phases oscillate along with the energy flow and reverse the internal motions at the turning points. Considering the other possible soliton triplet solution, the internal motion of the central pulse is changed due to the other corresponding relation between the fringe and the variable $(\tau_{23}, \varphi_{23})$. This possible solution can be obtained from the first one through the mathematical property of autocorrelation. The variable $(\tau_{12}, \varphi_{12})$ can be also retrieved according to the consistency relations of $\tau_{12} + \tau_{23} = \tau_{13}$ and $\varphi_{12} + \varphi_{23} = \varphi_{13}$. It is found that both of the possible solutions are of vibrating dynamics, albeit with the opposite evolving directions of the central pulse.

In addition, we tune the laser settings to induce another type of vibrating soliton triplet near the regime of the equally spaced soliton triplet. Figures 4(a) and 4(b) show the 2D contour plots of the real-time spectral interferograms and their calculation results of the first-order autocorrelation traces, respectively. Oscillating structures are clearly observed in the close-up of the spectral interferograms [Fig. 4(c)], indicating the recurrent motion of the central pulse and the tailing pulse. We first analyze the fringes of $(\tau_{12}, \varphi_{12})$ and $(\tau_{23}, \varphi_{23})$. The close-up illustrated in Fig. 4(d) displays an interleaved fringe pattern. Similarly, we first investigate one possible soliton triplet

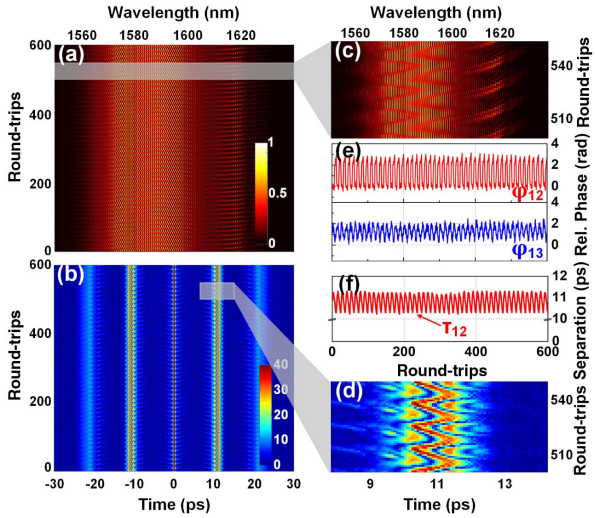

Fig. 4. Vibrating equally spaced soliton triplet. (a) 2D contour plot of the shot-to-shot spectra; (b) 2D contour plot of the shot-to-shot first-order autocorrelation traces; (c), (d) close-ups of the spectra and autocorrelation traces; (e) retrieved relative phases of the central pulse (top panel) and tailing pulse (bottom panel); (f) retrieved temporal separation of the central pulse.

solution by retrieving the variable $(\tau_{12}, \varphi_{12})$. It is found that the central pulse is characterized by vibrating motion. Compared to the case illustrated in Fig. 3, the central pulse seems to be trapped and vibrate in the vicinity of the center line (corresponding to $\tau_{12} = \tau_{23}$), undergoing the attractive and repulsive forces induced by the leading and tailing pulses. Oscillating temporal separation and relative phase are retrieved as shown in the top panel of Figs. 4(e) and 4(f). The central pulse reverses the internal motion at each turning point, which validates the vibrating dynamics within the soliton triplet. Next, the fringe of $(\tau_{13}, \varphi_{13})$ is analyzed to feature the internal motion of the tailing pulse with respect to the leading pulse. Limited by the low contrast of this fringe, we just retrieve the relative phase as depicted in the bottom panel of Fig. 4(e). Obvious phase oscillation is identified, and the evolving fringe implies an oscillating temporal motion of the tailing pulse. Hence, both the central pulse and the tailing pulse vibrate within the soliton triplet with the identical period. Especially, the central pulse is of more severe motion than the tailing pulse and recurrently passes through the center line in consideration of the remarkable interleaved autocorrelation trace. Indeed, the soliton triplet vibration is interpreted as one kind of the quasi-stationary manners resulting from a supercritical Hopf-type bifurcation, which is also reminiscent of the recurrent timing jitters within molecules. For the other possible solution, the internal motion of the temporal separations and relative phases is also dominated by the vibrating dynamics.

C. Evolving Unequally Spaced Soliton Triplet

The aforementioned dynamic motion is observed near a specific regime of equally spaced soliton triplets. Considering a more universal tri-soliton form, we now gain access to the internal motion of unequally spaced soliton triplets. The spectral interferograms are 2D contour plotted in Fig. 5(a), characterized by three superimposed fringes. See the close-ups shown in Figs. 5(b) and 5(c); twofold oscillating structures with different periods are readily observed. Figure 5(d) presents the calculated shot-to-shot first-order autocorrelation traces. Considering the gain dynamics, the temporal distribution is usually prone to be dense in the front part of the soliton molecule and sparse in the latter part. Accordingly, the retrieved relative phases are shown in the top, center, and bottom panels of Fig. 5(e). The insets present the close-ups. Corresponding trajectories are pictured in the 2D interaction plane [Fig. 5(f)]. No obvious temporal motion is observed within this soliton triplet. Relative phase evolution dominates the internal dynamics. In particular, the leading pulse and the central pulse are of a stationary relation since the trajectory is just fixed in the vicinity of the starting point, while the tailing pulse is characterized by the identical relative phase evolution with respect to the other two pulses. The rapid relative phase oscillation with a period of ~6 round-trips is modulated by a slowly varying envelope with a period of ~800 round-trips. This multifold phase evolution should be ascribed to the superposition of multiple phase oscillations with different periods, recalling the shaking soliton pairs as theoretically predicted in Ref. [19]. The trajectories of $(\tau_{13}, \varphi_{13})$ and $(\tau_{23}, \varphi_{23})$ respectively evolve on the fixed orbits with temporal separations of 18.64 ps and 11.49 ps. The multifold relative phase oscillation can be clearly witnessed in

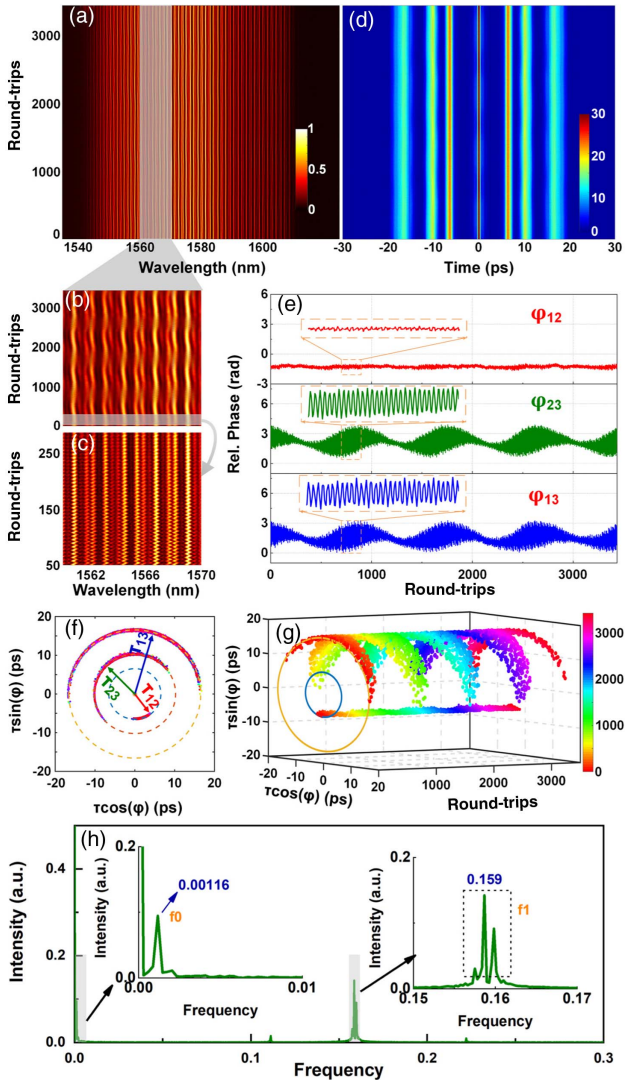

Fig. 5. Unequally spaced soliton triplet with oscillating phase. (a) 2D contour plot of the shot-to-shot spectra; (b), (c) close-ups of the spectra with different magnifications; (d) 2D contour plot of the shot-to-shot first-order autocorrelation traces; (e) retrieved relative phases of φ_{12}, φ_{23}, and φ_{13}, and the insets show the close-ups; (f) trajectories in the interaction plane; (g) trajectories of $(\tau_{12}, \varphi_{12})$ and $(\tau_{13}, \varphi_{13})$ in the interaction space; (h) oscillatory frequency of the phase evolution for the shaking soliton molecule.

the 3D interaction space [Fig. 5(g)]. The trajectory of $(\tau_{23}, \varphi_{23})$ features a dense oscillation and a large envelope. The turning points are no longer fixed at the same point in the interaction space but regulated by the slowly varying envelope. As a contrasting case, the trajectory of $(\tau_{12}, \varphi_{12})$ evolves in a confined region, which agrees with the stationary relation between the leading pulse and the central pulse. Furthermore, the oscillatory frequency is introduced to verify the internal dynamics of the shaking soliton molecules. The oscillatory frequency, in units of inverse round-trips, is calculated as illustrated in Fig. 5(h) by fast Fourier transforming the relative phase evolution [the bottom panel in Fig. 5(e)]. This multifold phase evolution can be resolved into three principal phase oscillations and some faint ones. Particularly, multiple closely spaced frequency peaks

existing near f_1 of 0.159 correspond to the rapid phase oscillation. Meanwhile, a lower frequency peak at f_0 of 0.00116 represents the slow phase oscillation, which regulates the rapid phase oscillation with a slowly oscillating envelope. The superposition of all the frequency peaks dominates the modulation of the oscillation amplitude. Intrinsically, the multifold internal motions should be attributed to the intricate energy oscillation of the tailing pulse as illustrated in Ref. [19]. This shaking soliton molecule mainly involves several rapid phase oscillations superimposed on a slowly vibrating motion.

The unequally spaced multi-soliton complex is essentially an asymmetric system in the sense that different temporal separations may impose on the binding strengths within molecules. Especially as illustrated in Fig. 5, the closely spaced leading and central pulses are tightly bound together to form a stationary soliton pair with a separation of ~7.24 ps. Behaving as a single pulse entity, this soliton unit is further bound with another tailing pulse over a large temporal separation of ~18.64 ps. The oscillating phase declares a relatively loosely bound state between the soliton pair and the tailing pulse. This soliton triplet can therefore be described as a $2+1$ soliton molecule [43]. The interactions can be classified into the intramolecular bond and the intermolecular bond with different binding strengths. The soliton pair sustained by the strong bond is robust towards the external perturbations, while the intermolecular bond is weak so that the tailing pulse may approach the soliton pair to form a more stable tri-soliton system or inversely escape from the bond and wander as an independent singlet. Particularly, the adjustment of pump power can impose on the evolution within molecules by varying their binding strengths.

Finally, another type of unequally spaced soliton triplet is presented with both temporal motion and relative phase evolution. Shown in Fig. 6(a) are the shot-to-shot spectral interferograms, yielding stepping fringes towards longer wavelengths. Figure 6(b) presents the corresponding first-order autocorrelation traces. The retrieved temporal separations and relative phases of (τ_{12}, φ_{12}) and (τ_{13}, φ_{13}) are respectively illustrated in Figs. 6(c) and 6(d). In accordance with the aforementioned analysis, the leading pulse and the central pulse constitute the bound state without intramolecule evolution, interpreted as a stationary soliton pair. The trajectory of (τ_{12}, φ_{12}) is limited in a confined region in the interaction space as depicted in Fig. 6(e). Referring to the soliton pair, the tailing pulse is of weaker bond than the case in Fig. 5, exhibiting a recurrent flipping motion and stepping phase evolution. It is also validated by the visualization shown in the interaction space. In particular, each step is triggered by a burst flipping motion of the tailing pulse, accompanied with a rapid phase progression and a small back-drift. After the burst process, the temporal separation remains constant and the relative phase mildly increases until the next step. The tailing pulse keeps trying to break away from the soliton pair, but the attractive force from the pair is strong enough to pull it back, creating a dynamic equilibrium. Especially, gain saturation dynamics play a crucial role in this step-like phase evolution.

To further verify the internal motion of the triplet with stepping phase evolution, we provide the analytical fit for the typical soliton triplets with stepping phase evolution according to

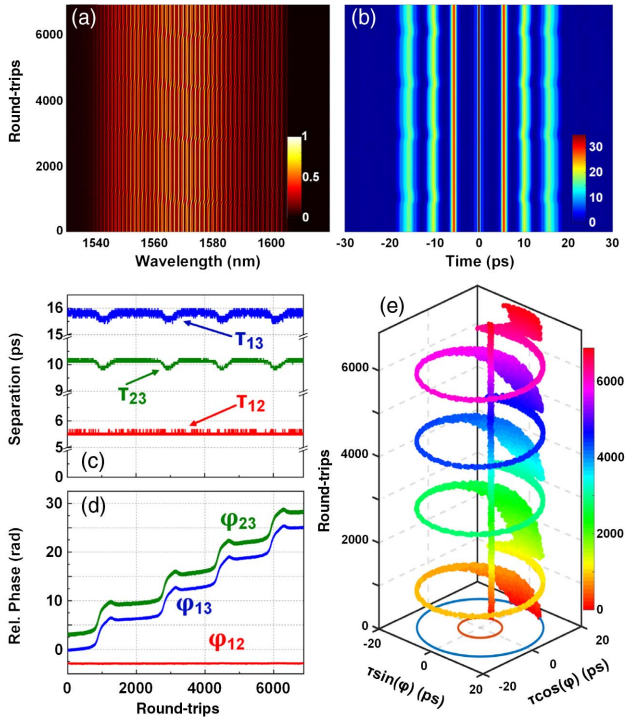

Fig. 6. Unequally spaced soliton triplet with stepping phase evolution. (a) 2D contour plot of the shot-to-shot spectra; (b) 2D contour plot of the shot-to-shot first-order autocorrelation traces; (c) retrieved temporal separations of τ_{12}, τ_{23}, and τ_{13}; (d) retrieved relative phases of φ_{12}, φ_{23}, and φ_{13}; (e) trajectories of (τ_{12}, φ_{12}) and (τ_{13}, φ_{13}) in the interaction space.

the method in Ref. [42]. Particularly, the leading pulse is set as the reference with a fixed pointing direction. Then we consider a constant relative phase ($\varphi_{12} = -\pi$) and temporal separation ($\tau_{12} = 5.5$ ps) between the leading pulse and central pulse according to the experimental results (presented as Fig. 6). In addition, the periodical burst flipping motion of the tailing pulse is also introduced in the analytical fit. The temporal separations between each constituent are shown in Fig. 7(a). The stepping phase evolution between the leading pulse and tailing pulse is modelled by the simple equation

$$\varphi_{13} = \cos(z) + z - 1, \tag{1}$$

where $z = n/70 \cdot \pi$, n being the round-trip number. The relative phases between pulses are shown in Fig. 7(b). We stress that each soliton of the triplet is chosen to have a Gaussian profile with a temporal width of 100 fs. As the temporal distribution shown in Fig. 7(c), the leading pulse and the central pulse constitute the bound state without intramolecule evolution, interpreted as a stationary soliton pair. Referring to the soliton pair, the tailing pulse is of weaker bond, exhibiting recurrent oscillating motion and stepping phase evolution. Based on these parameters, we model the spectral intensity evolution over 600 round-trips in Fig. 7(d), yielding stepping fringes towards longer wavelength. Moreover, the oscillating motion of the tailing pulse can be also identified in the spectral fringes. The corresponding first-order autocorrelation trace is depicted in Fig. 7(e). The oscillatory motions can be clearly observed in

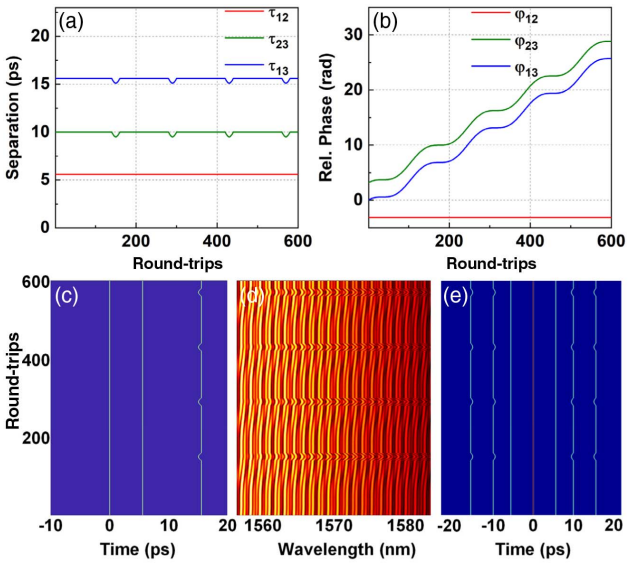

Fig. 7. Analytical fit for the soliton triplet with stepping phase evolution. (a) Evolution of the temporal separations and (b) the relative phases between constituents of the triplet; (c) temporal distribution; (d) corresponding evolution of the spectral intensity profile; (e) corresponding first-order autocorrelation trace.

the corresponding fringes. This simple analytical description of the temporal separations and phase evolution convincingly reproduces the results in Fig. 6, confirming the interpretation of the dynamic pulse structure as an unequally spaced soliton triplet with stepping phase evolution.

4. CONCLUSION

To summarize, we detailedly characterize the transient dynamics of soliton triplets in a dispersion-managed fiber laser by using the DFT technique. Beyond the most fundamental level of soliton pairs, soliton molecules with more constituents have more degrees of freedom because of the pulse separations and relative phases. Considering a triplet form of leading, central, and tailing pulses, two classes of soliton triplets are highlighted. Near the equally spaced regime, vibrating motions of the central and tailing pulses are captured. The soliton triplet vibration exhibits oscillating temporal separations and relative phases. Further insights unveil different binding strengths in the general unequally spaced soliton triplets, interpreted as $2+1$ soliton molecules. The intramolecular bond forms the stationary soliton pair behaving as an entity within the triplets. The intermolecular bond yields fixed and periodically evolving temporal separations of the tailing pulse, respectively accompanied with oscillating and stepping relative phase evolution. All these findings can spread new perspectives into real-time molecule dynamics with more degrees of freedom and highlight the possible application for all-optical bit storage.

Funding. National Natural Science Foundation of China (61775067, 61775072); Ministry of Education—Singapore (MOE2019-T1-001-111); National Research Foundation Singapore (NRF-CRP-18-2017-02).

Disclosures. The authors declare no conflicts of interest.

†These authors equally contributed to this work.

REFERENCES

1. N. J. Zabusky and M. D. Kruskal, "Interaction of 'solitons' in a collisionless plasma and the recurrence of initial states," Phys. Rev. Lett. **15**, 240–243 (1965).
2. L. F. Mollenauer, R. H. Stolen, and J. P. Gordon, "Experimental observation of picosecond pulse narrowing and solitons in optical fibers," Phys. Rev. Lett. **45**, 1095–1098 (1980).
3. G. I. Stegeman and M. Segev, "Optical spatial solitons and their interactions: universality and diversity," Science **286**, 1518–1523 (1999).
4. D. R. Solli, C. Ropers, P. Koonath, and B. Jalali, "Optical rogue waves," Nature **450**, 1054–1057 (2007).
5. P. Grelu and N. Akhmediev, "Dissipative solitons for mode-locked lasers," Nat. Photonics **6**, 84–92 (2012).
6. N. Akhmediev and A. Ankiewicz, "Dissipative solitons: from optics to biology and medicine," in *Lecture Notes in Physics* (Springer, 2008).
7. G. Z. Zhao, X. S. Xiao, J. W. Mei, and C. X. Yang, "Multiple dissipative solitons in a long-cavity normal-dispersion mode-locked Yb-doped fiber laser," Chin. Phys. Lett. **29**, 034207 (2011).
8. D. Y. Tang, L. M. Zhao, B. Zhao, and A. Q. Liu, "Mechanism of multisoliton formation and soliton energy quantization in passively mode-locked fiber lasers," Phys. Rev. A **72**, 043816 (2005).
9. D. Y. Tang, B. Zhao, L. M. Zhao, and H. Y. Tam, "Soliton interaction in a fiber ring laser," Phys. Rev. E **72**, 016616 (2005).
10. M. Pang, W. He, X. Jiang, and P. St. J. Russell, "All-optical bit storage in a fibre laser by optomechanically bound states of solitons," Nat. Photonics **10**, 454–458 (2016).
11. B. A. Malomed, "Bound solitons in the nonlinear Schrödinger–Ginzburg–Landau equation," Phys. Rev. A **44**, 6954–6957 (1991).
12. N. N. Akhmediev, A. Ankiewicz, and J. M. Soto-Crespo, "Multisoliton solutions of the complex Ginzburg-Landau equation," Phys. Rev. Lett. **79**, 4047–4051 (1997).
13. D. Y. Tang, W. S. Man, H. Y. Tam, and P. D. Drummond, "Observation of bound states of solitons in a passively mode-locked fiber laser," Phys. Rev. A **64**, 033814 (2001).
14. L. Gui, X. Xiao, and C. Yang, "Observation of various bound solitons in a carbon-nanotube-based erbium fiber laser," J. Opt. Soc. Am. B **30**, 158–164 (2013).
15. J. Peng, L. Zhan, S. Luo, and Q. Shen, "Generation of soliton molecules in a normal-dispersion fiber laser," IEEE Photonics Technol. Lett. **25**, 948–951 (2013).
16. Y. Luo, J. Cheng, B. Liu, Q. Sun, L. Li, S. Fu, D. Tang, L. Zhao, and D. Liu, "Group-velocity-locked vector soliton molecules in fiber lasers," Sci. Rep. **7**, 2369 (2017).
17. Y. Luo, Y. Xiang, B. Liu, Y. Qin, Q. Sun, X. Tang, and P. Shum, "Manipulation of dispersion-managed soliton molecules in a near zero-dispersion fiber laser," IEEE Photon. J. **10**, 7105210 (2018).
18. Y. Wang, D. Mao, X. Gan, L. Han, C. Ma, T. Xi, Y. Zhang, W. Shang, S. Hua, and J. Zhao, "Harmonic mode locking of bound-state solitons fiber laser based on MoS_2 saturable absorber," Opt. Express **23**, 205–210 (2015).
19. J. M. Soto-Crespo, P. Grelu, N. Akhmediev, and N. Devine, "Soliton complexes in dissipative systems: vibrating, shaking, and mixed soliton pairs," Phys. Rev. E **75**, 016613 (2007).
20. A. Zavyalov, R. Iliew, O. Egorov, and F. Lederer, "Dissipative soliton molecules with independently evolving or flipping phases in mode-locked fiber lasers," Phys. Rev. A **80**, 043829 (2009).
21. B. Ortaç, A. Zaviyalov, C. K. Nielsen, O. Egorov, R. Iliew, J. Limpert, F. Lederer, and A. Tünnermann, "Observation of soliton molecules with independently evolving phase in a mode-locked fiber laser," Opt. Lett. **35**, 1578–1580 (2010).
22. M. A. Abdelalim, Y. Logvin, D. A. Khalil, and H. Anis, "Steady and oscillating multiple dissipative solitons in normal-dispersion mode-locked Yb-doped fiber laser," Opt. Express **17**, 13128–13139 (2009).

23. A. Mahjoubfar, D. V. Churkin, S. Barland, N. Broderick, S. K. Turitsyn, and B. Jalali, "Time stretch and its applications," Nat. Photonics **11**, 341–351 (2017).
24. G. Herink, B. Jalali, C. Ropers, and D. R. Solli, "Resolving the build-up of femtosecond mode-locking with single-shot spectroscopy at 90 MHz frame rate," Nat. Photonics **10**, 321–326 (2016).
25. J. Peng, M. Sorokina, S. Sugavanam, N. Tarasov, D. V. Churkin, S. K. Turitsyn, and H. Zeng, "Real-time observation of dissipative soliton formation in nonlinear polarization rotation mode-locked fibre lasers," Commun. Phys. **1**, 20 (2018).
26. Y. Y. Luo, Y. Xiang, T. Liu, B. Liu, R. Xia, Z. Yan, X. Tang, D. Liu, Q. Sun, and P. P. Shum, "Real-time access to the coexistence of soliton singlets and molecules in an all-fiber laser," Opt. Lett. **44**, 4263–4266 (2019).
27. X. Liu and Y. Cui, "Revealing the behavior of soliton buildup in a mode-locked laser," Adv. Photon. **1**, 016003 (2019).
28. X. Liu, D. Popa, and N. Akhmediev, "Revealing the transition dynamics from *Q* switching to mode locking in a soliton laser," Phys. Rev. Lett. **123**, 093901 (2019).
29. X. Liu and M. Pang, "Revealing the buildup dynamics of harmonic mode-locking states in ultrafast lasers," Laser Photon. Rev. **13**, 1800333 (2019).
30. J. Peng and H. Zeng, "Build-up of dissipative optical soliton molecules via diverse soliton interactions," Laser Photon. Rev. **12**, 1800009 (2018).
31. H. J. Chen, M. Liu, J. Yao, S. Hu, J. B. He, A. P. Luo, W. C. Xu, and Z. C. Luo, "Buildup dynamics of dissipative soliton in an ultrafast fiber laser with net-normal dispersion," Opt. Express **26**, 2972–2982 (2018).
32. A. F. J. Runge, N. G. R. Broderick, and M. Erkintalo, "Observation of soliton explosions in a passively mode-locked fiber laser," Optica **2**, 36–39 (2015).
33. Y. Yu, Z. Luo, J. Kang, and K. K. Y. Wong, "Mutually ignited soliton explosions in a fiber laser," Opt. Lett. **43**, 4132–4135 (2018).
34. Z. W. Wei, M. Liu, S. X. Ming, A. P. Luo, W. C. Xu, and Z. C. Luo, "Pulsating soliton with chaotic behavior in a fiber laser," Opt. Lett. **43**, 5965–5968 (2018).
35. Y. Q. Du, Z. W. Xu, and X. W. Shu, "Spatio-spectral dynamics of the pulsating dissipative solitons in a normal-dispersion fiber laser," Opt. Lett. **43**, 3602–3605 (2018).
36. J. M. Soto-Crespo, M. Grapinet, P. Grelu, and N. Akhmediev, "Bifurcations and multiple-period soliton pulsations in a passively mode-locked fiber laser," Phys. Rev. E **70**, 066612 (2004).
37. M. Liu, A. Luo, Z. Luo, and W. Xu, "Dynamic trapping of a polarization rotation vector soliton in a fiber laser," Opt. Lett. **42**, 330–333 (2017).
38. K. Krupa, K. Nithyanandan, U. Andral, P. Tchofo-Dinda, and P. Grelu, "Real-time observation of internal motion within ultrafast dissipative optical soliton molecules," Phys. Rev. Lett. **118**, 243901 (2017).
39. X. Liu, X. Yao, and Y. Cui, "Real-time observation of the buildup of soliton molecules," Phys. Rev. Lett. **121**, 023905 (2018).
40. M. Liu, H. Li, A. Luo, H. Cui, W. Xu, and Z. Luo, "Real-time visualization of soliton molecules with evolving behavior in an ultrafast fiber laser," J. Opt. **20**, 034010 (2018).
41. G. Herink, F. Kurtz, B. Jalali, D. R. Solli, and C. Ropers, "Real-time spectral interferometry probes the internal dynamics of femtosecond soliton molecules," Science **356**, 50–54 (2017).
42. Z. Q. Wang, K. Nithyanandan, A. Coillet, P. Tchofo-Dinda, and P. Grelu, "Optical soliton molecular complexes in a passively mode-locked fibre laser," Nat. Commun. **10**, 830 (2019).
43. P. Grelu and N. Akhmediev, "Group interactions of dissipative solitons in a laser cavity: the case of 2+1," Opt. Express **12**, 3184–3189 (2004).